# Scalable Electromagnetic Energy Harvesting Using Frequency-Selective Surfaces

Faruk Erkmen, *Graduate Student Member, IEEE*, Thamer S. Almoneef, *Member, IEEE*, and Omar M. Ramahi, *Fellow, IEEE*

***Abstract*— We present a frequency-selective surface (FSS) that is specially designed and optimized for ambient RF energy harvesting. The unit cell geometry incorporates channeling features in order to combine the collected power from multiple unit cells, allowing for efficient operation under low-power conditions. To demonstrate its performance, we designed and fabricated a matched full-wave rectifier integrated with the absorber FSS. Radiated measurements for the complete rectenna system are included in this paper demonstrating strong agreement with the simulation results. The proposed periodic structure absorbs 97% of the available energy at its resistive load, thus making it an ideal candidate for energy harvesting and channeling applications. Overall Radiation-to-dc conversion efficiency of the fabricated prototype was measured to be 61% when the collected power at the rectifier was 15 dBm.**

***Index Terms*— Circuit analog absorber (CAA), electromagnetic (EM) energy harvesting, frequency-selective surfaces (FSSs), full-wave rectification, rectenna array, wireless power transfer (WPT).**

## I. Introduction

PERIODIC structures and electromagnetic (EM) absorbers have been widely used in various applications such as radar cross section reductions, EM interference/EM compatibility suppression, and anechoic chamber design [1]–[3]. The common goal across all the applications is to absorb the incident EM wave and minimize the reflections. Salisbury screens were the first radar absorber design with resistive sheets placed quarter wavelength above a ground plane [4]. Later, Jaumann absorbers were introduced expanding the absorption bandwidth using dielectrics and additional resistive sheets [5]. In subsequent years, other materials, such as ferrite tiles, lossy dielectrics, pyramidal absorbers, and carbon nanotubes, have been used in absorber designs [6]–[10]. Introduction of frequency-selective surfaces (FSSs) and circuit analog absorbers (CAAs) made it possible to produce complex impedance surfaces through the use of periodic structures, which resulted in enhanced bandwidth and lower profile absorbers [2], [11]–[13]. CAAs consist of specially designed periodic structures backed by a conductive surface. They can be modeled as transmission lines seen by the incident plane wave [14]–[18]. The CAAs use patterned periodic structures that can be modeled with lumped elements such as resistors, capacitors, and inductors. The lumped elements are defined in relation to the physical structure and the conductive ground plane is modeled as a short termination of the transmission line [5], [19], [20].

Absorbing the incident EM wave is the first step in a successful rectenna operation. In this regard, CAAs have very much in common with EM energy harvesting systems. However, energy harvesting also requires the absorbed energy to be transferred to a rectifier and converted into dc at the resistive load. Most of the previously published FSS works focused on the absorption characteristics only [1], [16], [17]. Dielectric losses were reported to be the key factor in absorbing and dissipating the energy in most cases [18], [21], [22]. Since power absorbed in the dielectric cannot be transferred to the rectifier, such FSS designs are not suitable for energy harvesting. Even though some designs used lumped resistors in periodic structures, the main focus has always been the absorption characteristics and bandwidth enhancement [1], [16], [17]. More recently, near unity absorption at lumped resistors has been achieved by metasurfaces [18], [23]. However, these designs only demonstrated how the EM energy was captured by the periodic surface; they did not study how the captured energy can be efficiently transferred to a rectifier. The conceivable next step for the earlier designs is to replace the resistors and employ rectifiers in each unit cell. However, given the size of the unit cells and available ambient RF power densities, the collected power would be very low, resulting in very low conversion efficiencies in the rectifiers [24]–[28]. Furthermore, a dc combiner circuit is needed to collect the power from each unit cell, adding further losses [29]. Antenna arrays have been used for wireless power transfer (WPT) applications before, but these were not periodic absorbing surfaces; they were designed for retrodirective antenna solutions with improved bandwidth and scanning capabilities [30], [31].

Only very recently, FSSs have been used for energy harvesting and have been integrated with rectifiers [32], [33]. However, these designs also implemented rectifiers in every unit cell, which meant a considerable part of the collected power was dissipated at the diodes. Hence, the overall efficiency of the previous work was 25% and 50% at −6- and −10-dBm input power to the rectifiers, respectively [32], [33]. In this paper, we utilize an FSS-based design to address the channeling problem and to increase the overall rectenna efficiency. We first present the design of a planar and low-profile absorber surface based on the principles of FSSs. The surface consists of periodic structures with built-in

Manuscript received June 16, 2017; revised September 19, 2017 and December 7, 2017; accepted January 6, 2018. *(Corresponding author: Omar M. Ramahi.)*

F. Erkmen and O. M. Ramahi are with the Department of Electrical and Computer Engineering, University of Waterloo, Waterloo, ON N2L3G1, Canada (e-mail: oramahi@uwaterloo.ca).

T. S. Almoneef is with the Department of Electrical Engineering, Prince Sattam bin Abdulaziz University, Al-Kharj 11942, Saudi Arabia (e-mail: talmoneef@uwaterloo.ca).

Color versions of one or more of the figures in this paper are available online at http://ieeexplore.ieee.org.

Digital Object Identifier 10.1109/TMTT.2018.2804956

channeling features. We then design and integrate a full-wave bridge rectifier that has an input impedance matched to the load required by the FSS. Eliminating the matching network in WPT systems has been demonstrated before by directly matching the rectifier to the antenna [34], [35]. Overall efficiency of the structure reaches 61%, which was obtained at 15-dBm input power at the rectifier. However, it should be noted that relatively high input power of the rectifier is remedied by combining multiple unit cells of the FSS structure, resulting in a viable solution for RF energy harvesting in very low ambient power densities. We provide simulation results validated by experimental data, demonstrating the highly efficient radiation-to-dc conversion characteristics of the overall structure. We conclude by discussing the results and limitations of the proposed absorber surface.

## II. Absorber FSS Design

EM fields in uniform regions and waveguides have been modeled using uniform transmission lines [19]. These models provide very useful physical insight while offering clues to designing better and simpler FSS geometries [5]. For EM energy harvesting, our goal was to design a planar FSS that collects almost all of the available energy and channels it to a resistive load. Therefore, we used the traditional FSS design steps but optimized the structure for this specific goal. Although FSSs can be modeled as various configurations, series $RLC$ network was shown to be the best topology in terms of absorption and bandwidth and thus this approach was adopted in this paper [20].

In transmission line models, metallic strips perpendicular to the $E$-field of the incident plane wave were modeled as capacitance, whereas metallic strips parallel to the $E$-field of the incident plane wave have been modeled as inductance [19]. Therefore, two patch structures facing each other in a unit cell can compose a shunt $LC$ equivalent circuit [2], [13], [16], [17], [36], [37]. With the addition of a lumped resistor in between, the resulting dipole-like structure can be modeled as an $RLC$ network in the transmission line model. We used CST Microwave Studio to perform parametric EM simulations of the dipole structure. We used Rogers RO4003C as the PCB substrate and optimized the dimensions of the unit cell geometry at the design frequency of 2.45 GHz. Channeling traces were added as a design feature extending from one periodic boundary to the other, so that any number of unit cells in a row could be continuously connected to each other. The lumped resistor was strategically connected between the channeling traces, enabling parallel connection of the unit cells. A 3-D model of the optimized FSS unit cell is shown in Fig. 1(a), and the detailed dimensions of the unit cell geometry are provided in Fig. 1(b). Using a 1.524-mm substrate and a 5-mm air spacer, the overall height of the optimized structure was only 6.524 mm, which is less than 1/18th of the wavelength at the design frequency.

The absorption characteristics of the proposed design were simulated using periodic boundary conditions and Floquet ports in CST. The FSS structure was optimized for a linearly polarized plane wave incidence, as shown in Fig. 1(c). Accordingly, the simulation and measurement results in

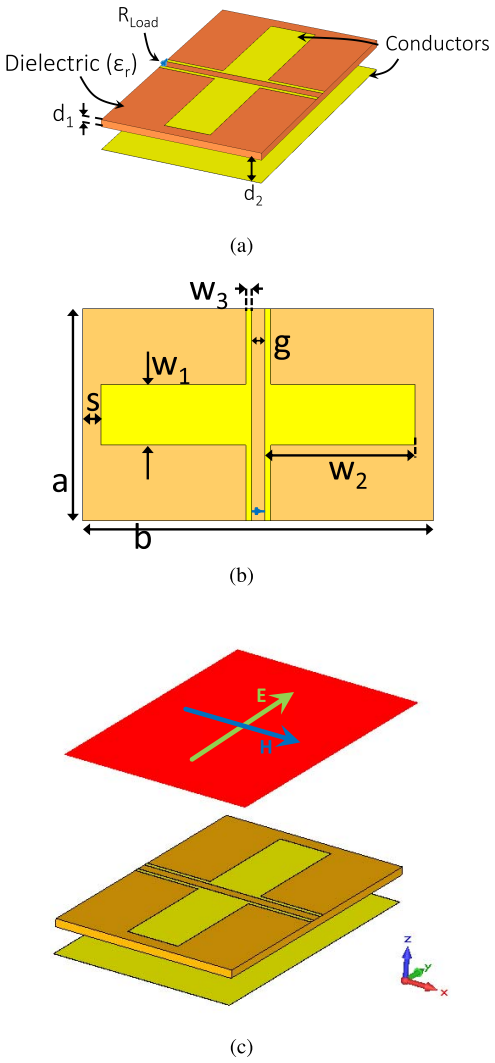


Fig. 1. Unit cell of the absorber FSS. (a) 3-D view. Dielectric substrate: RO4003C with 35-$\mu$m copper cladding, $\epsilon_r = 3.55$, $d_1 = 1.524$ mm, $d_2 = 5$ mm, and $R_{\text{Load}} = 370\ \Omega$. (b) Dimensions in mm. $a = 34.9$. $b = 57.5$. $s = 3$. $w_1 = 10$. $w_2 = 24.7$. $w_3 = 1$. $g = 2.1$. (c) Polarization of the incident plane wave.

this paper assume linearly polarized incident waves with properly aligned $E$-field vectors. Since the objective is energy harvesting rather than communication, there is no cross-polarization concerns in this particular rectenna system. However, polarization losses can be expected if the incident wave is not linearly polarized or if the $E$-field vector is not aligned with the FSS structure. As can be seen from the power flow diagram in Fig. 2(a), the accepted power by the unit cell is evidently concentrated on the channeling traces and almost entirely collected on the lumped resistor. The percentage of the incident power that is accepted by the FSS is provided in Fig. 2(b), and the distribution of the accepted power is provided in Fig. 2(c). Simulation results of the periodic structure in CST revealed that 98.5% of the incident power is absorbed by the FSS at 2.45 GHz, 97% is absorbed by the lumped resistor, 1.1% is absorbed by the dielectric substrate, and 0.4% is dissipated as metallic loss. Fig. 2(d) shows the impact of resistor location on the overall

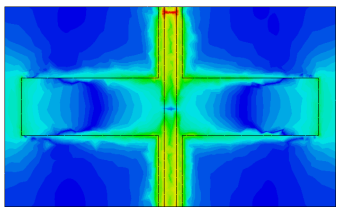

(a)

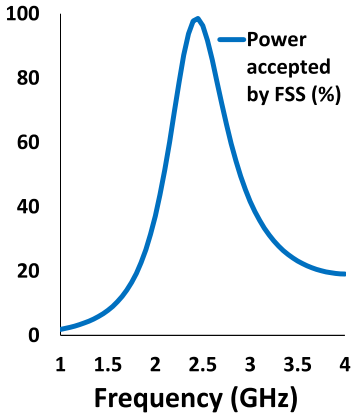


(b)

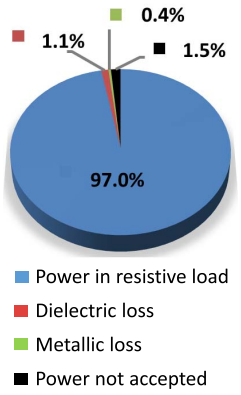


(c)

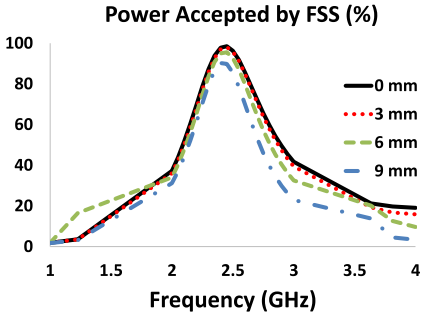


(d)

Fig. 2. Absorption characteristics of the FSS. (a) Power flow diagram of the unit cell. The highest red intensity (color version) corresponds to $1.6 \times 10^6$ W/m$^2$ and the highest blue intensity corresponds to 0 W/m$^2$. (b) Absorption characteristics versus frequency. (c) Distribution of the accepted power. (d) Impact of the resistor location on the overall FSS performance.

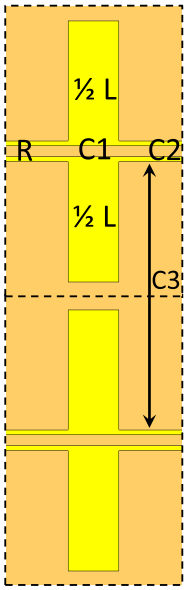


(a)

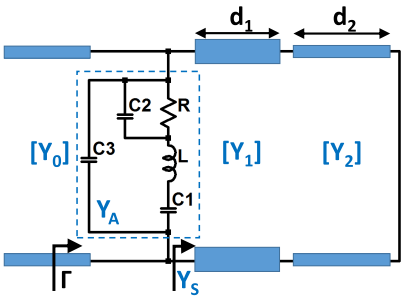


(b)

Fig. 3. (a) Description of the equivalent circuit model on unit cell geometry. (b) Schematic of the equivalent circuit with the lumped element values of $R = 370\ \Omega$, $L = 6.9$ nH, $C1 = 2.7$ pF, $C2 = 0.03$ pF, $C3 = 0.46$ pF, $Y_0 = 1/377$ S, $Y_1 = 1/200$ S, $Y_2 = 1/377$ S, $d_1 = 1.524$ mm, and $d_2 = 5$ mm.

FSS performance. Various offset positions of the resistor from the proposed location were simulated, and the results indicate that the FSS unit cell is not overly sensitive to the exact load location as long as the load is between the channeling traces.

A plane wave impinging on the FSS absorber was modeled with a transmission line equivalent circuit. Fig. 3(a) shows two adjacent unit cells and indicates the key physical features of the periodic structure as they correspond to the equivalent circuit components in Fig. 3(b). The interaction between the two unit cells is also represented in the circuit model. $Y_0$ denotes the free space admittance of 1/377 S, $Y_1$ denotes the characteristic admittance of the transmission line equivalent of the RO4003C substrate, and $Y_2$ denotes the characteristic admittance of the transmission line equivalent of the air spacer between the substrate and the conductive backing. The equivalent circuit of the proposed FSS unit cell was modeled with lumped elements. $L$ and $C1$ represent the dipole arms, $R$ represents the lumped resistor between the channeling traces, $C2$ represents the capacitance introduced by the two channeling traces within the unit cell, and $C3$ accounts for the capacitance introduced by the channeling traces between adjacent cells. RO4003C substrate with $d_1 = 1.524$ mm and $\epsilon_r = 3.55$ was modeled as a transmission line with electrical length of 8.6° and characteristic admittance of $\sqrt{\epsilon_r}/377 = 1/200$ S. An air spacer with $d_2 = 5$ mm was also modeled as a transmission line with the electrical length of 15° and characteristic admittance of 1/377 S. The reflection coefficient of the equivalent transmission line circuit model in Fig. 3(b) can be written as [20]

$$\Gamma = \frac{Y_0 - (Y_S + Y_A)}{Y_0 + (Y_S + Y_A)} \tag{1}$$

where $Y_0$, $Y_A$, and $Y_S$ are the admittances of free space, the equivalent circuit of the FSS, and the short-circuited transmission line, respectively. $\Gamma$ is the reflection coefficient.

In its simplest form, a CAA requires a resistive sheet of 377 Ω to match the free space impedance for ideal absorption. In practice, however, applications may demand different absorption levels, which, in turn, determine the equivalent resistance required from the CAA [20]. To obtain near unity absorption, a 370-Ω load resistor was used in our design. The lumped element values in the equivalent circuit were first estimated by using the relations given in [19] and then optimized using advanced design system (ADS) optimization tools. Fig. 4 provides a comparison of the FSS simulation

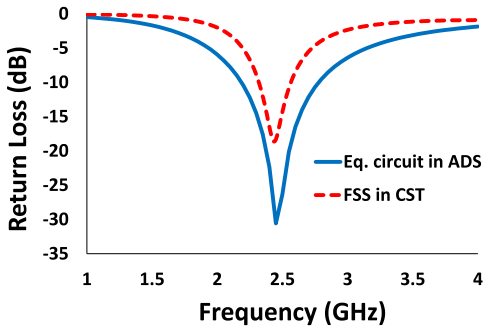


Fig. 4. Return loss of the absorber FSS. Full-wave EM simulation in CST compared with the equivalent circuit simulation in ADS.

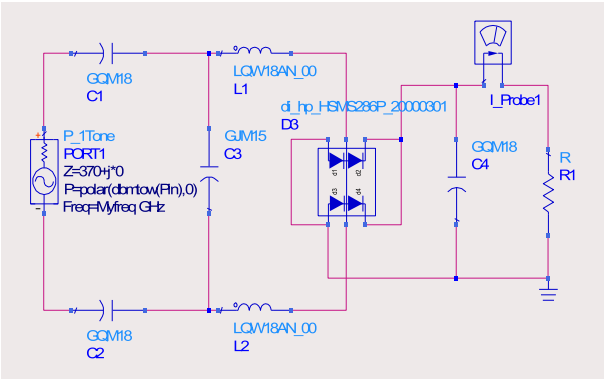


Fig. 5. Full-wave rectifier schematic in the ADS. $C1 = C2 = C4 = 100$ pF, $C3 = 0.3$ pF, $L1 = L2 = 12$ nH, and $R1 = 1$ kΩ.

in CST and its equivalent circuit simulation in the ADS. A very good agreement was obtained between the absorption characteristics of the two models, validating our physical interpretation of the unit cell geometry.

## III. Full-Wave Rectifier Design

A rectifier circuit can be constructed using a single-series-mounted diode, a single-shunt-mounted diode, or a diode bridge [38]. Among these, the single-diode configurations serve as half-wave rectifiers, which are the most common implementations due to its simple and low-cost construction [39]–[42]. However, half-wave rectifiers are limited to using only one half cycle of the input ac signal. Diode bridge rectifier, on the other hand, realizes full-wave rectification by taking advantage of both half cycles of the input ac signal, which can lead to improved efficiencies [34], [43], [44]. Full-wave rectification has a fewer examples compared with half wave [45], [46]. This is mainly because it requires two diodes to be turned ON for each half cycle, making it more suitable for higher power applications. The proposed FSS structure addresses the high input power limitation. Multiple unit cells in a row can be grouped together and feed the rectifier to obtain maximum efficiency. Therefore, a full-wave bridge rectifier is the chosen topology in this paper.

A detailed analysis of a bridge rectifier for 2.45 GHz was provided in [43]. We used a similar approach with a simplified matching circuit. Fig. 5 provides the ADS schematic

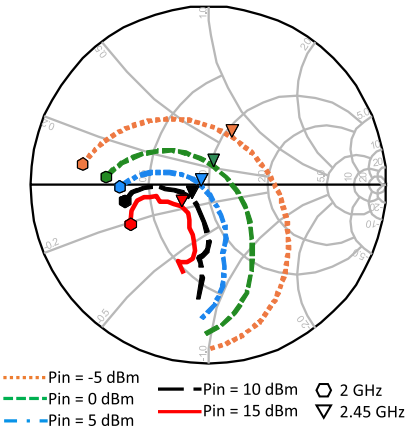


Fig. 6. Input impedance of the full-wave rectifier (matched to 370 Ω) at various input power levels. Frequency range is 2–3 GHz.

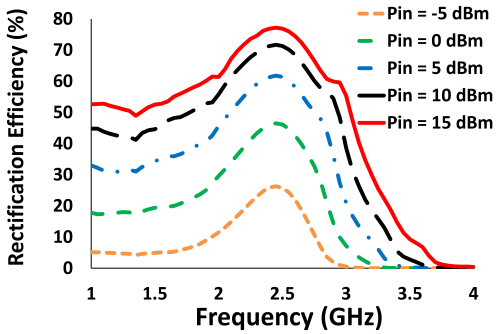


Fig. 7. Rectification efficiency of the rectifier ($\eta_{ac-dc}$) versus frequency at various input power levels.

of the full-wave rectifier circuit. HSMS-286P (by Broadcom, formerly Avago) was used as the quad bridge rectifier that consists of four Schottky diodes. $C1$ and $C2$ are dc blocking capacitors. $C3$, $L1$, and $L2$ are matching network components. $R1$ is the output load resistor and $C4$ is the smoothening capacitor to minimize output ripples. Murata capacitors and inductors were preferred with the component families and values provided in Fig. 5.

Using Broadcom component library for HSMS-286P, we used a large-signal S-parameter solver of the ADS and matched the input impedance of the rectifier to 370 Ω. The matching components were particularly selected from commercially available discreet values. The entire schematic was then simulated using the manufacturers' component libraries. Fig. 6 shows the impedance matching of the rectifier. Excellent matching was obtained over a wide input power range.

Fig. 7 shows the rectification efficiency of the rectifier versus frequency at various input power levels, and Fig. 8 provides the effect of the load $R1$ on the rectification efficiency. The results shown in Figs. 7 and 8 are consistent with similarly designed full-wave rectifiers in the literature [43], [44]. Here, the rectification efficiency is defined as

$$\eta_{ac-dc} = \frac{P_{dc}}{P_{ac}} \tag{2}$$

where $P_{dc}$ is the power at the rectifier load resistor and $P_{ac}$ is the input power at the rectifier input terminals. Although the

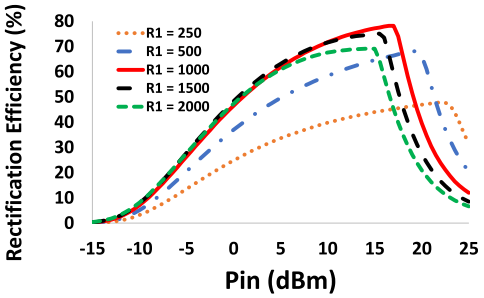


Fig. 8. Rectification efficiency of the rectifier ($\eta_{\text{ac-dc}}$) versus load resistor ($R1$) value.

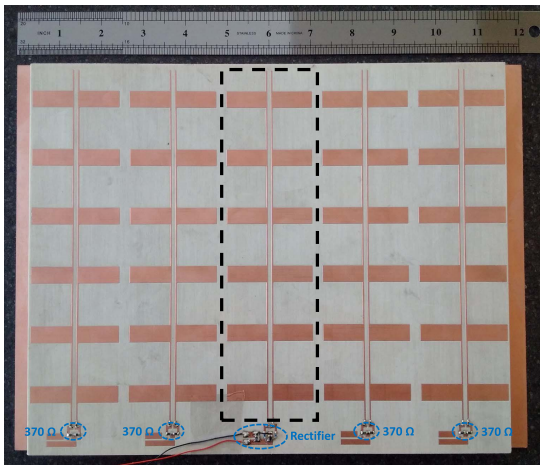


Fig. 9. Fabricated FSS absorber integrated with full-wave rectifiers on an RO4003C substrate mounted 5 mm above a copper plate. Marked rectangle: physical area of the measured row.

efficiency in Fig. 7 is steadily increasing with higher input power, it is very important to note that this trend does not continue after 15 dBm, where the rectifier reaches its peak efficiency. For input powers more than 15 dBm, the impedance match of the rectifier deteriorates and the efficiency becomes dramatically lower. A harmonic balance solver of the ADS was used to determine the input power dependence of the rectification efficiency, which is provided together with the measurement results in Section IV.

## IV. Results and Discussion

The proposed FSS absorber was fabricated on an RO4003C substrate with 1.524-mm thickness and 35-$\mu$m copper cladding, as shown in Fig. 9. An RO4003C board was 228.6 mm $\times$ 304.8 mm, which was enough area to print $5 \times 6 = 30$ unit cells. The full-wave rectifier layout was also printed at the end of each row, integrated to the continuous channeling traces. As discussed later in this section, this configuration combines the collected power from six unit cells and feeds into the rectifier. The center row was used for radiated measurements while others were terminated with 370-$\Omega$ resistors. Nylon spacers of 5 mm height (with negligible permittivity) were used to elevate the FSS substrate above a conducting plane of 228.6 mm $\times$ 304.8 mm. One of the main limitations of the previous FSS-based energy harvesting

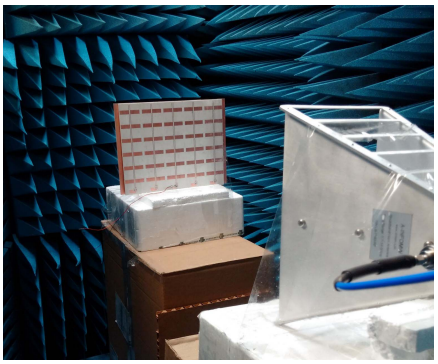

Fig. 10. Measurement setup inside an anechoic chamber.

systems was the need to implement individual rectifiers on each unit cell of the periodic structure. This resulted in lower efficiencies due to the small size of the EM collectors (i.e., the unit cells). In this paper, we utilized the channeling traces to combine the collected energy from multiple unit cells into a single rectifier. This approach makes it possible to increase the electrical size of the EM collector and hence the power collected per rectifier.

Overall performance of the rectenna was evaluated using the radiation-to-dc power conversion efficiency defined as

$$\eta_{\text{Rad-dc}} = \frac{P_{\text{dc}}}{P_{\text{Rad}}} \tag{3}$$

where $P_{\text{dc}}$ is the power at the load resistor and $P_{\text{Rad.}}$ is the total incident radiated power available at the physical area of the FSS row (enclosed by the dashed lines in Fig. 8) [34], [46]. $\eta_{\text{Rad-dc}}$ can be written as the product of three efficiencies

$$\eta_{\text{Rad-dc}} = \eta_{\text{Rad-ac}} \times \eta_{\text{Matching}} \times \eta_{\text{ac-dc}} \tag{4}$$

where $\eta_{\text{Rad-ac}}$ represents the radiation-to-ac efficiency and it indicates the percentage of the available radiated power that is captured by the FSS at its resistive load. $\eta_{\text{Matching}}$ is the matching efficiency, which indicates the percentage of the ac power that is actually delivered to the rectifier. $\eta_{\text{ac-dc}}$ represents the ac-to-dc conversion efficiency and it indicates the percentage of the available input RF power of the rectifier that is converted to dc power at the load. The simulation results of $\eta_{\text{Rad-ac}}$, $\eta_{\text{Matching}}$, and $\eta_{\text{ac-dc}}$ are given in Figs. 2(b), 6, and 7, respectively. In this section, we focus on the integrated system as a whole and measure the overall performance of the entire EM energy harvesting system. Radiation-to-dc conversion efficiency is a holistic metric for any rectenna system indicating what percentage of the available EM power (radiated) on a given surface area can be collected and converted into dc power at the system load.

A photograph of the measurement setup inside an anechoic chamber is shown in Fig. 10. A signal generator was used as the source. The output of the signal generator was amplified and fed into a standard gain horn antenna. The horn antenna was positioned such that the electric field of the incident wave on the FSS was parallel to the dipole arms. The FSS absorber was placed 1 m away from the horn antenna. Considering the design frequency of 2.45 GHz and the largest unit cell

TABLE I
LINK BUDGET PARAMETERS AT 2.45 GHz

| | |
|---|---|
| **Transmitter Parameters** | |
| Frequency ($f$) | 2.45 GHz |
| Source output power ($P_s$) | 2 dBm |
| Measured cable loss ($L_c$) | 1.8 dB |
| Amplifier gain ($G_a$) | 35.6 dB |
| Tx antenna (i.e. Horn) gain at 2.45 GHz ($G_h$) | 9.4 dB |
| EIRP ($P_s$-$L_c$+$G_a$+$G_h$) | 45.2 dBm |
| **Propagation Parameters** | |
| Distance ($d$) | 1 m |
| Free space path loss ($L_{fs}$) | 11 dB |
| RF power density at panel surface ($S_{Rad.}$) | 34.2 dBm/m$^2$ |
| RF power density at panel surface ($S_{Rad.}$) | 0.2635 mW/cm$^2$ |
| **Panel Parameters** | |
| Physical area of the FSS unit cell ($A_{uc}$) | 20.07 $cm^2$ |
| Physical area of the row with 6 unit cells ($A_p$) | 120.41 $cm^2$ |

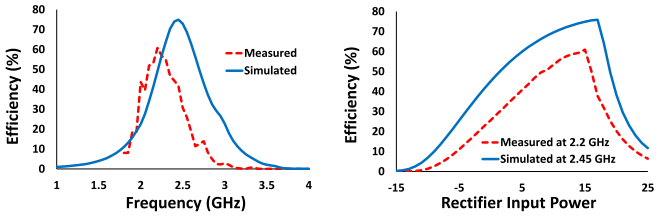


(a) (b)

Fig. 11. Measured radiation-to-dc conversion efficiency of the FSS-based full-wave rectenna. (a) As a function of frequency. (b) As a function of rectifier input power.

dimension of 57.5 mm, the measurement distance of 1 m satisfied the far-field conditions. Measurements were carried out with varying incident power and frequency. The rectified dc voltage across the load was recorded using a digital multimeter, and the collected dc power, $P_{\text{dc}}$, was calculated for all test cases.

To obtain the efficiency in (3), the available incident power $P_{\text{Rad.}}$ was determined by applying the link budget calculations [34], [46]

$$P_{\text{Rad.}} = S_{\text{Rad.}}\ A_p \tag{5}$$

$$S_{\text{Rad.}} = \text{EIRP}\ \frac{1}{4\pi d^2} \tag{6}$$

$$\text{EIRP} = P_s - L_c + G_a + G_h \tag{7}$$

where EIRP is the effective isotropic radiated power of the transmitter, $A_p$ is the physical area of the FSS unit cell, and $L_{fs} = 1/4\pi d^2$ is the distance dependence or the free space path loss of the EM energy expressed with inverse square law. The source power $P_s$ was known from the signal generator. The losses of the coaxial cables were measured using an Agilent E-5071C vector network analyzer. The amplifier gain $G_a$ was measured with a power meter and the horn antenna gain $G_h$ was obtained from its datasheet. Table I provides the definitions of the link budget parameters and their values at 2.45 GHz. Available radiated power $P_{\text{Rad.}}$ was calculated to be 31.73 mW (15 dBm).

Fig. 11(a) shows the measured radiation-to-dc conversion efficiency as a function of frequency. Peak efficiency was measured as 61% at 2.2 GHz. That is, the proposed rectenna was able to convert 61% of the available radiated power at its surface into practical dc power at its load. We emphasize that this efficiency should not be compared with the widely reported RF-to-dc conversion efficiencies in the literature. The RF-to-dc conversion efficiency is a measure of the rectifier circuit only where the RF power is fed into the rectifier port (generally via an SMA connection), and the rectified dc power is measured at the load resistor. The recorded 61% efficiency in this paper includes receiving the EM radiation, transferring the captured power to the rectifier and converting it into dc power at the load. It should be noted that the incident radiated power used in the measurement setup was linearly polarized with properly aligned $E$-field vectors. True ambient power in real life can be composed of randomly polarized waves, which would degrade the overall rectenna efficiency.

Fig. 11(a) also shows the expected efficiency curve over the same frequency range based on the simulation results of the different efficiencies involved. The "simulated" trace is obtained by multiplying the simulation results of the subefficiencies from the previous sections [as defined in (4)]. Expected peak efficiency was 75% at 2.45 GHz. The lower measured efficiency and the frequency shift of 200 MHz can be mainly attributed to the finite size of the FSS and its ground plane. Optimized unit cell characteristics are fairly accurate for the central cells, but not for the ones at the periphery of the FSS panel. Thus, the peripheral cells could cause mismatches and distorted absorption characteristics, which would lead to lower efficiency and shifted frequency. Nevertheless, the recorded 61% efficiency is much higher than the previously reported FSS-based rectennas [32], [33].

Fig. 11(b) shows the radiation-to-dc conversion efficiency as a function of the incident power. The load voltage was recorded, as the source output was increased by 1-dBm steps. The ac-to-dc conversion efficiency of the full-wave rectifier in Section III was simulated as a function of rectifier input power using the harmonic balance solver of the ADS. The obtained results are in agreement with those obtained using the state-of-the-art rectifier designs for similar input power levels [43], [45], [46]. In order to compare our measurements with the simulation results, the RF power collected and delivered to the rectifier was calculated using the link budget equations (5)–(7). As shown in Fig. 11(b), the measurements show a very good agreement with the simulation results regarding the power dependence of the rectenna efficiency. Experimental results are lower than those of the simulations mostly due to the finite size of the FSS panel.

The limitations in Fig. 11(a) can be addressed with straightforward improvements. The frequency shift can be remedied by using a larger FSS panel to minimize the impact of peripheral unit cells. The bandwidth can be widened by optimizing the geometry for a lower resistor value for the FSS and matching the rectifier accordingly (albeit trading off absorption level). However, the power dependence in Fig. 11(b) stems from diode fundamentals and had been the main limitation of previously reported work [18], [23]. Rectifiers are nonlinear circuits and their characteristics depend on the input power. Rectification efficiency peaks over a limited range of the input power and gradually degrades outside that range.

TABLE II
REALIZED SCALABILITY

| Multi-cell configuration | Physical area multiplier (1 unit cell = 20.07cm$^2$) | Max. absorption efficiency | Equivalent effective area multiplier | Ambient power density required to collect 15dBm at the load |
|---|---|---|---|---|
| N=1 cell | 1 | 97% | 0.97 | 1.6244 mW/cm$^2$ |
| N=2 cells | 2 | 80% | 1.6 | 0.9848 mW/cm$^2$ |
| N=4 cells | 4 | 87% | 3.48 | 0.4528 mW/cm$^2$ |
| N=6 cells | 6 | 79% | 4.74 | 0.3324 mW/cm$^2$ |
| N=8 cells | 8 | 78% | 6.24 | 0.2525 mW/cm$^2$ |
| N=16 cells | 16 | 77% | 12.32 | 0.1279 mW/cm$^2$ |
| N=32 cells | 32 | 36% | 11.52 | 0.1368 mW/cm$^2$ |

Measurement results in Fig. 11 show that the proposed design is an excellent integrated rectenna at 15-dBm input power to the rectifier. In the fabricated panel, 6 unit cells were connected to the rectifier and from Table I, this meant that the peak efficiency was measured at a power density of 0.2635 mW/cm$^2$. However, the real life ambient RF power densities are lower than the experimental setup [24]–[27]. One way to address this limitation is to employ a rectifier that is highly efficient at very low input power levels and that can operate over a wide input power range. Unfortunately, the physical mechanisms of diodes make this solution almost impossible [28]. The alternative way to address the power dependence in Fig. 11(b) is to utilize larger EM collectors per rectifier so that even at low power densities, the collected energy can still feed the rectifier at its peak conversion efficiency. This is one of the key features of the proposed FSS design in this paper.

The scalable architecture of the proposed absorber is further demonstrated in Fig. 12(a), which shows how multiple cells can be connected to a common resistive load. Since the physical area of the multicell structure expands with the number of cells (i.e., $N$), the total available radiated power incident on its surface also increases by a factor of $N$. This means the resistive load can absorb up to $N$ times the power of a single cell. The concept was examined for $N = 1$, 2, 4, 6, 8, 16, and 32 cells using CST. The power flow diagrams and the absorption efficiencies are provided in Fig. 12(b) and (c), respectively. Simulation results are also summarized in Table II for comparison. The results indicate that the proposed FSS unit cell is indeed scalable but has some limitations. Absorption efficiency is highest for single unit cell at 97%, and it decreases as more cells are combined to the same load. However, even with lower efficiencies, the collected power at the load can increase significantly as the physical area gets larger. For example, the 16-cell configuration with 77% efficiency can collect more than 12 times the power of a single cell, clearly demonstrating the importance of a larger EM collector. The resistive load in these examples can be replaced with a matched rectifier, and the multicell rectenna can operate efficiently at much lower power densities than the levels required by a single unit cell rectenna. In terms of limitations, Table II shows that the absorbed power increases up to $N = 16$ cells. After this point, even doubling the physical area does not provide any net benefit in terms of absorbed power. Therefore, the concept is only applicable up to a certain number of cells. It was also observed that the absorption bandwidth becomes narrower, and the optimum load resistance deviates from 370 Ω as $N$ gets larger. We emphasize, however,

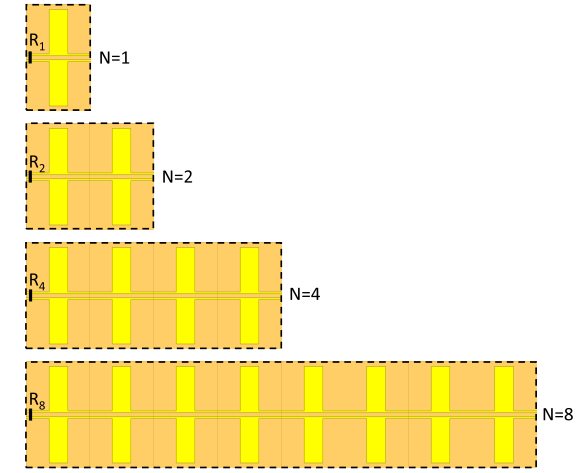


(a)

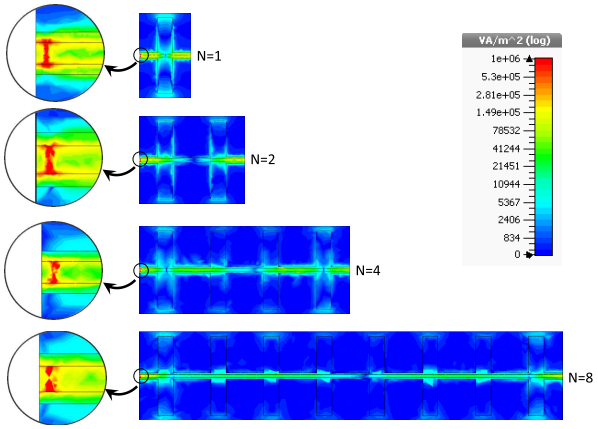


(b)

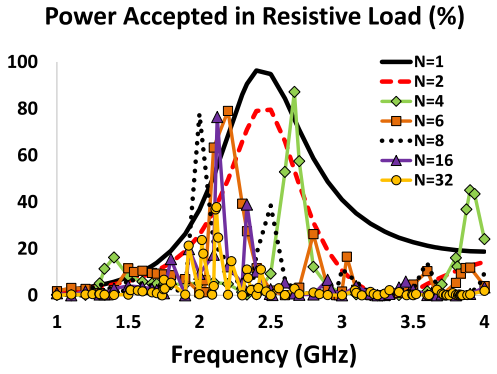


(c)

Fig. 12. Scalable architecture of the proposed FSS-based rectenna demonstrated. (a) Multiple cells in a row can be connected to a common resistive load; this is illustrated for $N = 1$, 2, 4, and 8 unit cells. (b) Power flow diagrams showing the majority of the absorbed power being concentrated on the resistive load. (c) Power absorbed by the resistive load as a percentage of the available incident power.

that the unit cell geometry in this paper was optimized for maximum absorption in a single-cell implementation. This objective can be relaxed in favor of scalability, by designing for more consistent bandwidth and load behavior.

## V. Conclusion

We presented an FSS absorber design that can be used for ambient RF energy harvesting or controlled WPT. The FSS unit cell was constructed with built-in channeling features to combine the collected power from multiple unit cells. We demonstrated the excellent absorption characteristics of the periodic structure with 97% of the available energy being captured on its load. We then integrated the FSS absorber with a matched full-wave rectifier. The complete rectenna prototype was fabricated and tested through radiated measurements. 61% radiation-to-dc power conversion efficiency was measured, which represents the combined efficiency of receiving the EM radiation, transferring the captured power to the rectifier and converting it into dc power at the load. We also discussed the scalability of the proposed FSS absorber and its limitations.

## References


[1] S. Ghosh, S. Bhattacharyya, and K. V. Srivastava, "Design, characterisation and fabrication of a broadband polarisation-insensitive multi-layer circuit analogue absorber," *IET Microw., Antennas Propag.*, vol. 10, no. 8, pp. 850–855, 2016.

[2] D. Kundu, A. Mohan, and A. Chakrabarty, "Thickness reduction of single layer circuit analog absorber," in *Proc. IEEE Appl. Electromagn. Conf. (AEMC)*, Dec. 2015, pp. 1–2.

[3] S. Ghosh, S. Bhattacharyya, D. Chaurasiya, and K. V. Srivastava, "A broadband polarization-insensitive circuit analog absorber using lumped resistors," in *Proc. IEEE Appl. Electromagn. Conf. (AEMC)*, Dec. 2015, pp. 1–2.

[4] W. Salisbury, "Absorbent body for electromagnetic waves," U.S. Patent 2 599 944 A, Jun. 10, 1952.

[5] B. Munk, *Frequency Selective Surfaces: Theory and Design*. Hoboken, NJ, USA: Wiley, 2005.

[6] F. Erkmen, C. C. Chen, and J. L. Volakis, "Impedance matched ferrite layers as ground plane treatments to improve antenna wide-band performance," *IEEE Trans. Antennas Propag.*, vol. 57, no. 1, pp. 263–266, Jan. 2009.

[7] F. Erkmen, C. C. Chen, and J. L. Volakis, "UWB magneto-dielectric ground plane for low-profile antenna applications," *IEEE Antennas Propag. Mag.*, vol. 50, no. 4, pp. 211–216, Aug. 2008.

[8] F. Erkmen, C.-C. Chen, and J. L. Volakis, "UWB low profile antennas using ferrite loaded GP," in *Proc. IEEE Antennas Propag. Soc. Int. Symp.*, Jul. 2008, pp. 1–4.

[9] M.-J. Park and S.-S. Kim, "Wide bandwidth pyramidal absorbers of granular ferrite and carbonyl iron powders," in *IEEE Int. Magn. Conf. (INTERMAG) Dig. Tech. Papers*, Apr. 2000, p. 457.

[10] I. H. Baek *et al.*, "Passive mode-locking of a Ti:Sapphire laser using low-dimensional carbon nanostructures," in *Proc. Quantum Electron. Conf. Lasers Elect.-Opt. (CLEO/IQEC/PACIFIC RIM)*, Aug. 2011, pp. 1154–1155.

[11] W.-H. Choi *et al.*, "Design of circuit-analog (CA) absorber and application to the leading edge of a wing-shaped structure," *IEEE Trans. Electromagn. Compat.*, vol. 56, no. 3, pp. 599–607, Jun. 2014.

[12] Q. Zhang and Z. Shen, "A dual-polarized switchable microwave absorber," in *Proc. IEEE Int. Symp. Antennas Propag.*, Jul. 2012, pp. 1–2.

[13] W. Che, H. Ye, Y. Xiong, Y. Chang, and C. Christopoulos, "A fast and efficient method for design of circuit analog absorbers consisting of resistive square loop arrays," in *Proc. IEEE Int. Conf. Comput. Electromagn.*, Feb. 2015, pp. 35–37.

[14] Y. Shang, S. Xiao, and Z. Shen, "A thin wideband circuit analog absorber using square-loop arrays," in *Proc. IEEE Antennas Propag. Soc. Int. Symp. (APSURSI)*, Jul. 2013, pp. 472–473.

[15] B. A. Munk, P. Munk, and J. Pryor, "On designing Jaumann and circuit analog absorbers (CA absorbers) for oblique angle of incidence," *IEEE Trans. Antennas Propag.*, vol. 55, no. 1, pp. 186–193, Jan. 2007.

[16] Y. Han, W. Che, C. Christopoulos, Y. Xiong, and Y. Chang, "A fast and efficient design method for circuit analog absorbers consisting of resistive square-loop arrays," *IEEE Trans. Electromagn. Compat.*, vol. 58, no. 3, pp. 747–757, Jun. 2016.

[17] D. Kundu, A. Mohan, and A. Chakrabarty, "Single-layer wideband microwave absorber using array of crossed dipoles," *IEEE Antennas Wireless Propag. Lett.*, vol. 15, pp. 1589–1592, 2016.

[18] S. Shang, S. Yang, J. Liu, M. Shan, and H. Cao, "Metamaterial electromagnetic energy harvester with high selective harvesting for left- and right-handed circularly polarized waves," *J. Appl. Phys.*, vol. 120, no. 4, p. 045106, 2016.

[19] N. Marcuvitz, *Waveguide Handbook*. London, U.K.: IET, 1951.

[20] A. K. Rashid, Z. Shen, and R. Mittra, "On the optimum design of a single-layer thin wideband radar absorber," in *Proc. IEEE Int. Symp. Antennas Propag. (APSURSI)*, Jul. 2011, pp. 2916–2919.

[21] Y. Z. Cheng, Y. Wang, Y. Nie, R. Zhou Gong, X. Xiong, and X. Wang, "Design, fabrication and measurement of a broadband polarization-insensitive metamaterial absorber based on lumped elements," *J. Appl. Phys.*, vol. 111, no. 4, p. 044902, 2012.

[22] S. Li, J. Gao, X. Cao, W. Li, Z. Zhang, and D. Zhang, "Wideband, thin, and polarization-insensitive perfect absorber based the double octagonal rings metamaterials and lumped resistances," *J. Appl. Phys.*, vol. 116, no. 4, p. 043710, 2014.

[23] T. S. Almoneef and O. M. Ramahi, "Metamaterial electromagnetic energy harvester with near unity efficiency," *Appl. Phys. Lett.*, vol. 106, no. 15, p. 153902, 2015.

[24] Z. Popović *et al.*, "Scalable RF energy harvesting," *IEEE Trans. Microw. Theory Techn.*, vol. 62, no. 4, pp. 1046–1056, Apr. 2014.

[25] R. Vyas, H. Nishimoto, M. Tentzeris, Y. Kawahara, and T. Asami, "A battery-less, energy harvesting device for long range scavenging of wireless power from terrestrial tv broadcasts," in *IEEE MTT-S Int. Microw. Symp. Dig.*, Montreal, QC, Canada, Jun. 2012, pp. 1–3.

[26] M. Pinuela, P. D. Mitcheson, and S. Lucyszyn, "Ambient RF energy harvesting in urban and semi-urban environments," *IEEE Trans. Microw. Theory Techn.*, vol. 61, no. 7, pp. 2715–2726, Jul. 2013.

[27] M. Pinuela, D. C. Yates, P. D. Mitcheson, and S. Lucyszyn, "London RF survey for radiative ambient RF energy harvesters and efficient DC-load inductive power transfer," in *Proc. 7th Eur. Conf. Antennas Propag. (EuCAP)*, Gothenburg, Sweden, Apr. 2013, pp. 2839–2843.

[28] C. H. P. Lorenz, S. Hemour, and K. Wu, "Physical mechanism and theoretical foundation of ambient RF power harvesting using zero-bias diodes," *IEEE Trans. Microw. Theory Techn.*, vol. 64, no. 7, pp. 2146–2158, Jul. 2016.

[29] U. Olgun, C. C. Chen, and J. L. Volakis, "Investigation of rectenna array configurations for enhanced RF power harvesting," *IEEE Antennas Wireless Propag. Lett.*, vol. 10, pp. 262–265, Apr. 2011.

[30] M. Ettorre, W. A. Alomar, and A. Grbic, "Long slot Van Atta array for far-field wireless power transfer," in *Proc. IEEE Int. Symp. Antennas Propag. USNC/URSI Nat. Radio Sci. Meeting*, San Diego, CA, USA, Jul. 2017, pp. 1291–1293.

[31] P. D. H. Re, S. K. Podilchak, S. Rotenberg, G. Goussetis, and J. Lee, "Retrodirective antenna array for circularly polarized wireless power transmission," in *Proc. 11th Eur. Conf. Antennas Propag. (EUCAP)*, Paris, France, Mar. 2017, pp. 891–895.

[32] S. Keyrouz, G. Perotto, and H. J. Visser, "Frequency selective surface for radio frequency energy harvesting applications," *IET Microw., Antennas Propag.*, vol. 8, no. 7, pp. 523–531, 2014.

[33] D. Ferreira, L. Sismeiro, A. Ferreira, R. F. S. Caldeirinha, T. R. Fernandes, and I. Cuiñas, "Hybrid FSS and rectenna design for wireless power harvesting," *IEEE Trans. Antennas Propag.*, vol. 64, no. 5, pp. 2038–2042, May 2016.

[34] F. Erkmen, T. S. Almoneef, and O. M. Ramahi, "Electromagnetic energy harvesting using full-wave rectification," *IEEE Trans. Microw. Theory Techn.*, vol. 65, no. 5, pp. 1843–1851, May 2017.

[35] M. Koohestani, M. Zhadobov, and M. Ettorre, "Design methodology of a printed WPT system for HF-band mid-range applications considering human safety regulations," *IEEE Trans. Microw. Theory Techn.*, vol. 65, no. 1, pp. 270–279, Jan. 2017.

[36] A. P. Sohrab and Z. Atlasbaf, "A circuit analog absorber with optimum thickness and response in X-band," *IEEE Antennas Wireless Propag. Lett.*, vol. 12, pp. 276–279, 2013.

[37] Y.-Q. Pang, Y.-J. Zhou, and J. Wang, "Equivalent circuit method analysis of the influence of frequency selective surface resistance on the frequency response of metamaterial absorbers," *J. Appl. Phys.*, vol. 110, no. 2, p. 023704, 2011.
[38] V. Marian, B. Allard, C. Vollaire, and J. Verdier, "Strategy for microwave energy harvesting from ambient field or a feeding source," *IEEE Trans. Power Electron.*, vol. 27, no. 11, pp. 4481–4491, Nov. 2012.
[39] H. Takhedmit, L. Cirio, F. Costa, and O. Picon, "Transparent rectenna and rectenna array for RF energy harvesting at 2.45 GHz," in *Proc. 8th Eur. Conf. Antennas Propag. (EuCAP)*, The Hague, The Netherlands, Apr. 2014, pp. 2970–2972.
[40] S. D. Assimonis and A. Bletsas, "Energy harvesting with a low-cost and high efficiency rectenna for low-power input," in *Proc. IEEE Radio Wireless Symp. (RWS)*, Newport Beach, CA, USA, Jan. 2014, pp. 229–231.
[41] J. Heikkinen and M. Kivikoski, "Low-profile circularly polarized rectifying antenna for wireless power transmission at 5.8 GHz," *IEEE Microw. Wireless Compon. Lett.*, vol. 14, no. 4, pp. 162–164, Apr. 2004.
[42] J. Heikkinen and M. Kivikoski, "A novel dual-frequency circularly polarized rectenna," *IEEE Antennas Wireless Propag. Lett.*, vol. 2, no. 1, pp. 330–333, Oct. 2003.
[43] M. Ito *et al.*, "High efficient bridge rectifiers in 100 MHz and 2.4 GHz bands," in *Proc. IEEE Wireless Power Transf. Conf. (WPTC)*, Jeju City, South Korea, May 2014, pp. 64–67.
[44] S. A. Rotenberg, P. D. H. Re, S. K. Podilchak, G. Goussetis, and J. Lee, "An efficient rectifier for an RDA wireless power transmission system operating at 2.4 GHz," in *Proc. 32nd General Assembly Sci. Symp. Int. Union Radio Sci. (URSI GASS)*, Montreal, QC, Canada, Aug. 2017, pp. 1–3.
[45] B. Merabet *et al.*, "A 2.45-GHz localized elements rectenna," in *Proc. 3rd IEEE Int. Symp. Microw., Antenna, Propag. EMC Technol. Wireless Commun.*, Beijing, China, Oct. 2009, pp. 419–422.
[46] M. K. Hosain, A. Z. Kouzani, M. F. Samad, and S. J. Tye, "A miniature energy harvesting rectenna for operating a head-mountable deep brain stimulation device," *IEEE Access*, vol. 3, pp. 223–234, 2015.

**Faruk Erkmen** (GS'16) received the B.Sc. degree (Hons.) in electrical engineering from the Middle East Technical University, Ankara, Turkey, in 2006, the M.Sc. degree in electrical engineering specializing in electromagnetics from The Ohio State University, Columbus, OH, USA, in 2008, and the M.B.A. degree in technology and finance from Wilfred Laurier University, Waterloo, ON, Canada, in 2013. He is currently pursuing the Ph.D. degree in electrical and computer engineering at the University of Waterloo, Waterloo, ON, Canada.

In 2006, he joined as a Graduate Research Associate with the ElectroScience Laboratory, The Ohio State University. He has over 10 years of research and development experience in the IT industry. Since 2012, he has been a project management professional. He has authored or co-authored several journal and conference papers. His current research interests include small antennas, low-profile ground planes for ultrawideband antennas, antenna miniaturization techniques, wireless power transfer, electromagnetic energy harvesting, frequency selective surfaces, rectennas, and nanoantennas.

Mr. Erkmen was the recipient of the Best Paper Award from the Antenna Measurements Techniques Association 2007 Meeting, St. Lois, MO, USA. He is a Registered Professional Engineer in Canada.

**Thamer S. Almoneef** (GS'10–M'12) received the B.S. degree in electrical and computer engineering from Dalhousie University, Halifax, NS, Canada, in 2009, and the M.A.Sc. and Ph.D. degrees in electrical and computer engineering from the University of Waterloo, Waterloo, ON, Canada, in 2012 and 2017, respectively.

In 2012, he was appointed as a Lecturer and was granted a scholarship from Prince Sattam Bin Abdulaziz University, Al-Kharj, Saudi Arabia, to pursue his Ph.D. studies, where he is currently an Assistant Professor with the Department of Electrical and Computer Engineering. He has authored or co-authored over 20 refereed journals and conference papers. His current research interests include antenna theory, metamaterials and its wide range of applications, metamaterial absorbers, electrically small resonators, rectennas, electromagnetic energy harvesting, and renewable energy.

**Omar M. Ramahi** (F'09) was born in Jerusalem, Palestine. He received the B.S. degrees (Highest Hons.) in mathematics and electrical and computer engineering from Oregon State University, Corvallis, OR, USA, and the Ph.D. degree in electrical and computer engineering from the University of Illinois at Urbana–Champaign, Champaign, IL, USA, in 1990.

He was with the Digital Equipment Corporation (now Hewlett-Packard), where he was a member of the Alpha Server Product Development Group. In 2000, he joined the Faculty of the James Clark School of Engineering, University of Maryland at College Park, College Park, MD, USA, as an Assistant Professor, and later as a tenured Associate Professor. With the University of Maryland at College Park, he was also a faculty member with the CALCE Electronic Products and Systems Center. He is currently a Professor with the Electrical and Computer Engineering Department, University of Waterloo, Waterloo, ON, Canada. He has authored or co-authored over 390 journal and conference technical papers on topics related to the electromagnetic phenomena and computational techniques to understand the same. He co-authored *EMI/EMC Computational Modeling Handbook* (First Edition: Kluwer, 1998; Second Edition: Springer-Verlag, 2001; and Japanese Edition in 2005).

Dr. Ramahi was a recipient of the 2004 University of Maryland Pi Tau Sigma Purple Cam Shaft Award, the Excellent Paper Award of the 2004 International Symposium on Electromagnetic Compatibility, Sendai, Japan, the 2010 University of Waterloo Award for Excellence in Graduate Supervision, and the IEEE Electromagnetic Compatibility Society Technical Achievement Award in 2012.